ARTICLE

# Effects of the methylammonium ion substitutions by 5-ammoniumvaleric acid in lead trihalide perovskite solar cell: A combined experimental and theoretical investigation

Received 00th January 20xx,
Accepted 00th January 20xx

DOI: 10.1039/x0xx00000x

Rodrigo Urzúa-Leiva*[a], Amir Narymany Shandy[b], Haibing Xie[b], Mónica Lira-Cantú*[b], Gloria Cárdenas-Jirón[c]

In the last decade, lead triiodide perovskite ($APbI_3$) (A: organic cation) solar cells (PSC) have been broadly studied due to its promising features related to the low cost, easy manufacturing process, and stability. Strategies to improve device stability include the application of technics such as compositional engineering of the cation of these halide perovskites, but it is still a complex task to find the right balance between stability and power conversion efficiency of materials and complete devices. In this work, we performed a combined study of five samples of the $[5\text{-}AVA_{(1-x)}MA_x]PbI_3$ (5-AVA: ammonium valeric acid and MA: methylammonium) with x=1.0, 0.75, 0.5, 0.25 and 0.0, using X-Ray diffraction (XRD) and UV-VIS spectroscopy measurements in combination with periodic density functional theory (DFT) based calculations. Our samples showed an optical bandgap of 1.58 eV and the coexistence of the two phases as observed by XRD analyses. Theoretical results of the bandgaps for the no mixed phases (x=1.0 and x=0.0) show good agreement with the experiment, obtaining bandgap values overestimated by 0.18 eV and 0.33 eV, respectively. A direct relation between the amount of 5-AVA ions in the samples and the stability of the phases was theoretically found, proved through the increment observed in the bandgap and the cohesive energy. We proposed a compositional strategy to the perovskites $[5\text{-}AVA_{(1-x)}MA_x]PbI_3$ with x values at most of 0.5, based on the small blue-shift and the low absorbance reduction of the spectrum curve, added to the small phase stabilization found.

## Introduction

In the last decade, scientific research that concerns with green power generation of electricity has experienced a growing demand for new materials and technologies to deal with global warming and become a real alternative to fossil fuels. In this context, the electricity produced by photovoltaic solar cells is an outstanding source of energy due to its abundance and eternal nature. The last biggest scientific breakthroughs in this area befall the year 2009, with the invention of the perovskite solar cells (PSCs),[1] going on a few years from 3.8% to 25.2% power conversion efficiency.[2-4] Others important benefits of the PSCs come from the low cost compared with conventional solar cells, associated with inexpensive materials, easy manufactured process and high stability reached using cross-linking additives[5] or compositional engineering.[6, 7] The most typical and studied PSC is methylammonium lead trihalide, $MAPbX_3$ (MA=methylammonium and X=$Cl^-$, $Br^-$, $I^-$) with excellent optoelectronic properties associated to large light absorption coefficients, optimal band-gaps, and large carrier diffusion lengths.[8-10] Despite the growing interest, the development of PSCs has not been free of major issues such as poor material stability under operational conditions[11-15] and toxicity due to the use of lead as a metallic center, the later has limited the deployment and commercialization of PSCs as a future PV technological solution.[16] Different strategies have been proposed to circumvent these problems, for example in a recent publication[17], several potential substituents for the replacement of lead such as Sn,[18] Ge,[19] and Sb,[20] among others, has been reviewed, reaching efficiencies of 8.4%, 3.2%, and 3.8%, respectively. On the other hand, the stability problems can be associated with intrinsic factors as the crystalline structure and chemical stability, as also as extrinsic factors as moisture, UV radiation, and thermal stress.[12, 13, 21-23] The correct combination of these two key aspects is necessary to reach new PSCs aligned with the spirit of green power generation. Moreover, in line with chemical stability, potential substituents of the organic part have also been addressed. The replacement of the cationic MA by different atoms or molecules has been intensely studied with favourable improvement in device stability, for example, formamidinium

[a] *Instituto de Ciencias Químicas Aplicadas, Facultad de Ingeniería, Universidad Autónoma de Chile, Av. Pedro de Valdivia 425, 7500912, Providencia, Santiago, Chile.*
[b] *Catalan Institute of Nanoscience and Nanotechnology (ICN2), CSIC, and the Barcelona Institute of Science and Technology (BIST), Bellaterra E-8193, Spain.*
[c] *Laboratory of Theoretical Chemistry, Faculty of Chemistry and Biology, University of Santiago de Chile (USACH), 9170022, Santiago, Chile.*
*Author to whom the correspondence should be addressed:
rodrigo.urzua@uautonoma.cl, monica.lira@icn2.cat
Electronic Supplementary Information (ESI) available: [details of any supplementary information available should be included here]. See DOI: 10.1039/x0xx00000x

(FA), Cesium (Cs) and 5-ammonium valeric acid (5-AVA) have been analysed.[24, 25] Han et al.,[26] made a significant contribution to the state of the art of PSCs by proposing a hole-conductor-free perovskite based on a mixed of MA and 5-AVA iodide with lead(II) iodide. The results showed that the crystalline structure is less pore defect, improved the $TiO_2$ scaffold contact, resulting in a longer exciton lifetime with a higher quantum yield efficiency and high stability in air ambient conditions compared to $MAPbI_3$. Later, Nazeeruddin et al.,[27] achieved a one-year stable perovskite solar cell using interface engineering precisely using the combination of MA and 5-AVA, confirming the appropriated use of 5-AVA has a substituent.[28] In the later work, the beneficial effect of applying two mesoporous oxide layers[28, 29] in combination with the use of 5-AVA dopants and the elimination of a hole transport layer, was suggested as the reasons behind the remarkable device stability. Relatively few computational investigations of mix MA/5-AVA lead trihalide have been performed[30, 31] and to the best of our knowledge, limited connection with experimental results have been shown.

In this work, we present an experimental and theoretical combined study of the global and molecular effects on a systematic increase of 5-AVA concentration in the preparation of perovskite $[5\text{-}AVA_{(1-x)}MA_x]PbI_3$ crystals. Moreover, from the theoretical point of view, we analyse the molecular and optical implications of the substitution of MA by 5-AVA ions using the framework of density functional theory (DFT) and the plane wave methods.

## Experiments and calculation methods

### Experimental details

The $[5\text{-}AVA_{(1-x)}MA_x]PbI_3$ samples of five phases from x=0 to 1, with intermediate values of 0.25, 0.50 and 0.75, were synthesized and analysed by XRD to study the crystalline quality and composition of the materials. Moreover, a bandgap determination via UV-VIS measurement in the five phases was performed. For the preparation of the $[5\text{-}AVA_{(1-x)}MA_x]PbI_3$ samples, $PbI_2$, MAI and 5-AVA were dissolved in a 1:4 mixture of dimethyl sulfoxide (DMSO) and dimethylformamide (DMF), with the respective variation of the molar ratio between 5-AVA and MAI. The Glass/FTO substrates were cleaned with Hellmanex/distilled water/acetone/ethanol in sequence using an ultrasonic bath. Just before the material deposition via Spin-Coating in the Glovebox, the samples were plasma-etched to increase the wettability of the sample surface. After the dynamic spin coating, the samples were heated for 20 minutes at 100 °C and taken out of the glovebox to perform measurements. The UV-VIS spectra were measured in a Cary 4000 UV-VIS Spectrometer with a wavelength spectrum from 200 to 800 nm. To minimize systematical errors, a Glass/FTO reference was measured and its baseline was subtracted from the data of the samples.

The XRD-analysis was performed with a 2-Theta range from 5 to 60 degrees including a glass/FTO substrate as reference.

### Theoretical details

At low temperature, the crystallographic phase of perovskite $MAPbI_3$ has orthorhombic symmetry, with the MA ion ordered in the unit cell as shown in Fig. 1. The well-defined position of MA ions in the crystallographic unit cell is useful to make the substitutions of these ions by 5-AVA ions and keep invariant the dipole moment of the unit cell. We use the crystalline structure reported by Baikie et. al. [32] as the starting point, where we apply a systematic substitution of MA ion coordinates by 5-AVA ion, using the same orientation of the native zwitterion. Following the experiment samples, a total of five different phases of $[5\text{-}AVA_{(1-x)}MA_x]PbI_3$ was theoretically modelled, with x taking values of 1.0, 0.75, 0.5, 0.25, and 0.0. We perform a constrained geometry optimization on these structures keeping all unit cell angles fix to conserve the symmetry. All geometry optimization calculations were based on DFT,[33] where the generalized gradient approximation of Perdew-Burke-Ernzerhof (PBE)[34] was used to represent the exchange and correlation energy of the electrons using the Quantum-Espresso code[35]. Semi-empirical van der Waals corrections were considered by the use of Grimme's D3 correction.[36] Moreover, the plane wave (PW) technique along with PAW[37] pseudopotential was employed, using an energy cutoff of 400 Ry with a uniform Monkhorst-Pack[38] scheme of 7-5-7 k-points grid to sampling the entire Brillouin zone. The convergence tolerance for the total energy and Hellmann–Feynman force during the structural relaxation was set to $10^{-5}$ eV and 0.01 eV/Å, respectively. To an easy identification of the calculation scheme, we denote this strategy of calculation as DFT-PW/PBE-D3.

On the other hand, accurate energy, band-structure, and DOS (density of states) were determined through a single point calculation in the previously optimized geometry using the ADF-BAND program.[39, 40] We study the scalar relativistic effects through the inclusion of ZORA formalism in an all-electron (AE) calculation of the already mentioned properties using also the functional PBE-D3 with a triple-ζ basis set. We denote this strategy of calculation as DFT-AE/PBE-D3.

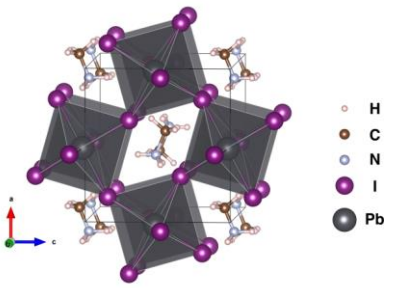


**Figure 1.** Schematic representation of the crystalline structure of the orthorhombic phase of $MAPbI_3$. A well-resolved position and orientation of MA ions are appreciable at this symmetry.

## RESULTS AND DISCUSSION

### Structural and UV-VIS characterization

The XRD analysis of the samples shows a good agreement with the already published XRD-properties of the perovskite,[41] as shown in Fig. 2. All peaks can be assigned either to the substrate (2θ=26.4º), an excess of $PbI_2$ (2θ=12.6º), or the phase $MAPbI_3$ (2θ= 14.8º, 20.1º and 24.5º).[42] The presence of $PbI_2$ is known to be beneficial for PSCs. Its passivation effect leads to the reduction of halide defect concentration (halide vacancies), resulting in longer carrier lifetime.[43] However, it can also result in inhibited charge transport and an increase in the degradation of the halide perovskite layer (due to the photodecomposition of $PbI_2$). To overcome this issue, the incorporation of organic additives or ligands, such as AVAi, helps to regulate the homogeneous distribution of $PbI_2$ in the halide perovskite thin film and to improve thin film properties.[44, 45] Thus, there is an optimal amount of AVAi concentration incorporated within the halide perovskite. As seen in Fig. 3, the optimal concentration of AVAi in the samples is at ~x=0.25 (for x in $[5\text{-}AVA_{(1-x)}MA_x]PbI_3$), above this value, the excess of $PbI_2$ is clearly observed by the increase of the $PbI_2$ peak at 12.6º.[42] This $MAPbI_3$-XRD pattern is then compared with the other $[5\text{-}AVA_{(1-x)}MA_x]PbI_3$ samples, as can be seen in Fig. 3. The very significant peaks for the 5-AVA containing samples at 5.8°, 7.8°, 9.4°, attributed to crystallographic planes of the formation of a 2D perovskite, are in good agreement with previously reported data,[26, 27] and can be assigned to $5\text{-}AVAPbI_3$.[46] It has previously suggested that the 5-AVAi, MAI and $PbI_2$ can form 2D Ruddlesden–Popper (RP) phases of $AVA_2(CH_3NH_3)_{n-1}Pb_nI_{3n+1}$ perovskite structure.[30] However, the concentration ratios used of each reactant are slightly different than the ones used in this work. Finally, we observe that the XRD pattern of the $[5\text{-}AVA_{(1-x)}MA_x]PbI_3$ (x = 0.25, 0.50, 0.75) show two sets of peaks, which can be assigned to either $MAPbI_3$ or $5\text{-}AVAPbI_3$. This indicates the coexistence of these two phases in the samples and is in good accordance with the results of UV-VIS analysis.

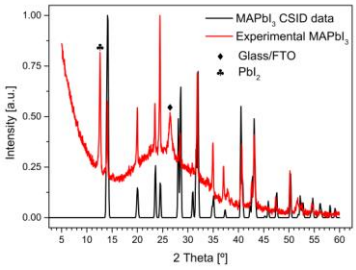


**Figure 2.** Comparison of the experimental XRD data with the published data of Yamada, Y et. al.[41] (CSID data) for $MAPbI_3$. All peaks can be assigned either to the perovskite, the substrate, or the $PbI_2$.

The UV-Vis absorption spectra, Fig. 4, show that $MAPbI_3$ achieved an optical bandgap of 1.58 eV, which agrees with others published works reporting bandgaps of ~1.6 eV,[47-50] making the reference samples of this series reliable. Analysing the UV-VIS spectra in Fig. 4, and starting from the $MAPbI_3$ reference absorption curve, we observe a consistent transition of the absorption peaks towards the optical bandgap of the $5\text{-}AVAPbI_3$ with an energy gap of 2.33 eV. The optical gap of the samples shows in Table 1, was estimated by the extrapolation of the linear region at the beginning of each absorption peak to the x-axis intercept, as indicated by the grey dashed lines in Fig. 4. On the other hand, Table 1 also shows the values of the principal absorptions bands obtained from the absorption curves derivatives (Fig. 1 Supporting Information). Two characteristic bands in the visible region of the spectra are appreciable in all samples containing a fraction of the MA cation, one at low energy and a second one at higher energy. The two bands have energies of ~1.6 eV and ~2.5 eV, respectively. The remaining sample, which contains only 5-AVA cation, confirms the absence of the first characteristic absorption band, suggesting that it is originated due to the effect of the MA ion on the cavity. Using theoretical calculations we analysed in more detail the effect of the MA and 5-AVA ions in the bands of the Fermi level frontier.

Table 1. Optical band-gap and principal absorption peak of the different phases of the $[5\text{-}AVA_{(1-x)}MA_x]PbI_3$ obtained from the UV-Vis absorption spectra and corresponding derivatives, respectively.

| $[AVA_{(1-x)}MA_x]PbI_3$ | Optical band-gap (eV) | Absorption peak (eV) |
|---|---|---|
| x=1 | 1.58 | 1.63 |
| x=0.75 | 1.59, 2.14 | 1.65, 2.47 |
| x=0.50 | 1.60, 2.25 | 1.66, 2.47 |
| x=0.25 | 1.59, 2.30 | 1.65, 2.46 |
| x=0 | 2.33 | 2.45 |

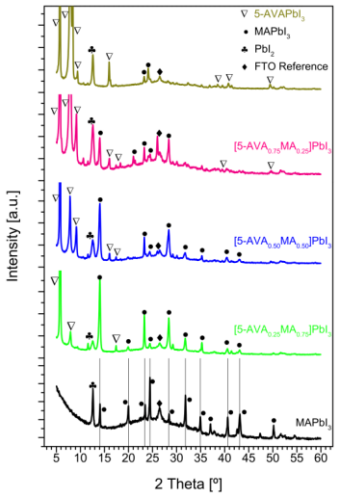


**Figure 3.** XRD analysis of the five $[5\text{-}AVA_{(1-x)}MA_x]PbI_3$ samples depending of the 5-AVAi content. The coexistence of the two phases, $MAPbI_3$ and $5\text{-}AVAPbI_3$, are verified by the observable phase transition between the two configurations.

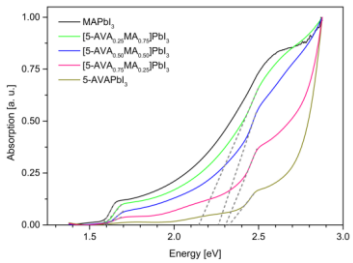


**Figure 4.** Absorption spectra of the different phases of the $[5\text{-AVA}_{(1-x)}\text{MA}_x]\text{PbI}_3$. Two optical transitions corresponding to bandgap energies of 1.58 eV and 2.33 eV for the $MAPbI_3$ and $5\text{-AVAPbI}_3$ respectively, can be observed.

### Theoretical results

Based on the optimized geometry of atomic coordinates and lattice parameters, and maintaining the lattice orthogonally fixed as discussed above, we found an excellent performance of the DFT-PW/PBE-D3 calculation scheme for reproducing the published crystallographic data. The experimental lattice parameters (a=8.836 Å, b=12.58 Å and c=8.555 ) used to compare our theoretical results in Fig. 5(a) was obtained from the ref.[32], determinates by single crystal X-ray diffraction at 100 K and structure solution using the Superflip algorithm. An additional lattice parameter from the ref.[51] was included in Fig. 5(a) as other sample to compare our results. The DFT-PW/PBE-D3 scheme of calculation only overestimates a maximum of 1.4 % of the lattice vector *a* in the $MAPbI_3$ phase. For the bandgap, we obtained a value of 1.7 eV, in agreement with reported values,[52, 53] showing not-dependency on the DFT-PW/PBE-D3 or DFT-AE/PBE-D3 scheme of calculation. In other words, the scalar relativistic effect considered at the DFT-AE/PBE-D3 scheme is negligible over this parameter. On the other hand, the obtained bandgap value, using the empirical dispersion correction D3, is 0.1 eV which is smaller than its counterpart (before correction), and although minimal, the volume of the unit cell is observed to be reduced. This result is in agreement with other published works,[52, 54] and indicates that for the appropriate treatment of the ionic interaction in this type of crystals, it is necessary to include some correction to the dispersion interactions.

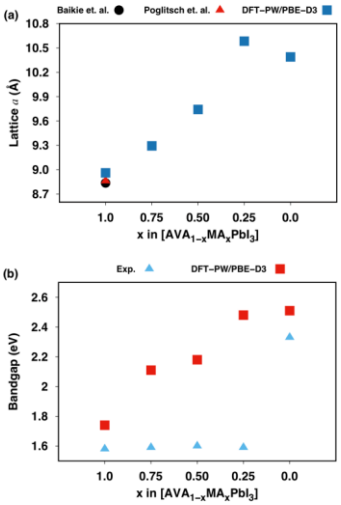


**Figure 5.** The behaviour of theoretically predicted lattice parameter *a* (a) and bandgap (b) in the different phases of $[5\text{-AVA}_{(1-x)}\text{MA}_x]\text{PbI}_3$ studied compared with the ref.[32] and ref.[51] in (a), and with our experimental values of $MAPbI_3$ phase in (b).

The systematic substitution of MA by 5-AVA ions in a single unit cell of the orthorhombic phase of $MAPbI_3$ shows a clear tendency over the size of lattice parameter *a* and the bandgap of the single crystal cell, finding both a direct relation with the increment of 5-AVA ions in the cell, as shown in Fig. 5. As expected, a large effect in the volume of the cell is appreciable, which is coherent with the increase of ionic radii values from 2.17 Å to 5.44 Å for MA and 5-AVA, respectively, calculated according to equations of Cheetham et. al.[55] The increase of the ionic radii is two times larger when MA is replaced by 5-AVA. As a results of the accommodation of this large new organic ion, the calculated bond distances of Pb-I in the quasi-octahedral $PbI_6$ is increased from 3.2 Å in the pure phase $MAPbI_3$ to more than 4.0 Å in the pure phase $AVAPbI_3$. This structural change has a direct relation with the large effect measured in the theoretical bandgap from the minimal substitution of MA by 5-AVA. From an energetic point of view, the calculated bandgaps show in Fig. 5(b) of the pure phases, $MAPbI_3$ (1.76 eV) and $5\text{-AVAPbI}_3$ (2.63 eV), are in good agreement with our experimental measures of the principal absorptions bands show in Table 1. However, the bandgaps calculated for the mixed phases (x=0.75, 0.5, and 0.25) have a very poor agreement with the measured experiment values. We can attribute this discrepancy to that the theoretical perovskite model used is based on the pure and infinitely periodic 3D orthorhombic structure of $MAPbI_3$, whereby construction the substitution of MA ions by 5-AVA is homogeneously replicated through the crystal. Large theoretical bandgap values are a result of the strong distortion of the octahedral $PbI_6$ structure due to the incorporation of AVA ions in the cavity of the MA ion. In contrast, as already explained, the samples analysed experimentally can present

subdomains corresponding to pure 3D and 2D perovskite (see Fig. 7 of the schematic model),[46] each with characteristic optical transitions observable in the spectrum, as shown in Fig. 4. For example, with a 1:4 ration for 5-AVA:MA ions, we can suppose a full substitution of MA ion only in the surfaces unit cell or close to them, and not substitution in the bulk of the crystal (Fig. 7b). Our experiment reflects well this phenomenon, as previously discussed, showing the two characteristic absorption bands in the mixed samples. Nevertheless, the theoretical bandgaps show the mixed samples transition to the full substituted 5-AVA unit cell, with a systematic increment of the bandgap value 1.74 eV <2.11 eV <2.18 eV <2.48 eV <2.51 eV in the same order that the substitution index increment of 5-AVA in the $[5\text{-AVA}_{(1-x)}\text{MA}_x]\text{PbI}_3$ samples. We attribute the increase of the bandgaps to a stabilization of the frontier conduction bands (valence band and conduction band) associated mainly to the formation of unoccupied orbitals from the 5-AVA ion closed to the Fermi level, as shown in Fig. 7c. Another important energetic aspect associated with the stability of the cell is the value of the cohesive energy. The calculated cohesive energy of the five phases was performed following the procedure developed by Yong-Hyon et al.[54] Fig. 6 shows that the cohesive energy is in line with the values reported for $\text{MAPbI}_3$, and also agree with the experimental results on the gain in the stability of perovskite crystal by partial substitution of MA ions by 5-AVA ions. In contrast to what we might think about the adverse effect on stability due to the strong structural distortion caused by the ionic radius of 5-AVA, the stability of the unit cell is favoured, being even 1.8 eV higher in the phase 5-$\text{AVAPbI}_3$ in comparison with the one of $\text{MAPbI}_3$. This result is also related to the increase of the bandgaps values, as previously discussed.

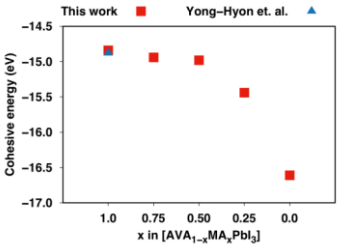


**Figure 6.** Calculated cohesive energy for the different phases of $[5\text{-AVA}_{(1-x)}\text{MA}_x]\text{PbI}_3$ compared with the work of ref [51].

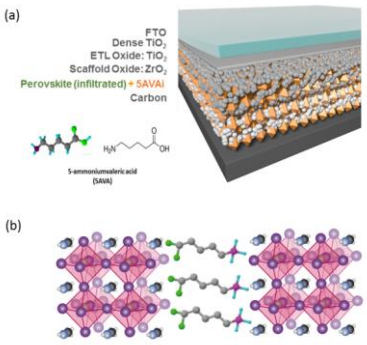


**Figure 7.** (a) Schematic representation of a Carbon-based Perovskite solar cell where the perovskite is introduced by infiltration. (b) Schematic representation of the AVAi molecule an its interaction with the MA halide perovskite.

From an electronic structure point of view, the DOS and pDOS of $\text{MAPbI}_3$ in the vicinity of Fermi level, shows a typical distribution also observed in other published works.[56-58] The valence bands maximum (VBM) is mainly on the iodide atoms and the conduction bands minimum (CBM) belong to lead atoms, as shown in Fig. 8a. Also, the orbital projections of these bands respond to typical *p*-character in both iodide and lead atoms of $\text{MAPbI}_3$ crystal (see Fig. 8b). On the other hand, in this phase of perovskite, the MA bands are negligible in the frontier of the Fermi level. Thus, once the systematic substitution of MA by 5-AVA takes place, a rearrangement of the frontier bands in all cases is observed (Fig. 2 Supporting Information), being mostly appreciable in the CB edge. In the case when MA is completely substituted, the CB edge mainly localized over Pb atoms in the $\text{MAPbI}_3$ phase, changes to localization on the 5-AVA ion with mostly *p*-character bands, in 5-$\text{AVAPbI}_3$ phase (see Figs. 8c and 8d). In contrast, the VB edge is almost unaffected by the substitution, with a minimal occurrence of 5-AVA states closed to the frontier of the Fermi level. The presence of metallic Pb in halide perovskites, indicates that Pb is unsaturated and thus, iodine deficiencies may also be present in the perovskite lattice of the reference sample.[59] This implies that the application of additives, such as AVAI, can effectively suppress the formation of metallic Pb via either direct electron donation to unsaturated Pb or immobilization of iodine as already reported.[44, 45] Additionally, our theoretical results show an increment of the PbI distances with the inclusion of 5-AVA ions in the unit cell, resulting in a most favourable interaction of 5-AVA ions with the unsatured Pb atoms, appreciable through the appearance of 5-AVA states in the CBM, as shown in Fig. 8(c). A qualitative description of these bands in the frontier region is shown in Fig. 3 of Supporting Information.

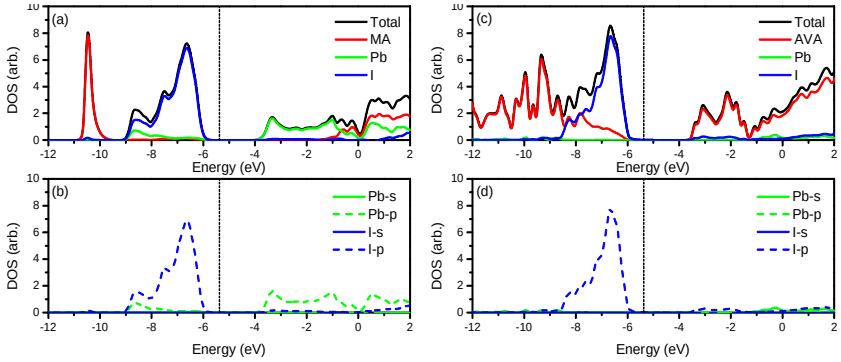


**Figure 8.** DOS and pDOS calculated at DFT-AE/PBE-D3 level of theory for the phases $MAPbI_3$ (a) and (b), and 5-$AVAPbI_3$ (c) and (d). For a better appreciation, pDOS is separated by atoms (Pb,I) and orbital (s,p).

The optical properties, in particular, the imaginary part of the dielectric constant ($\varepsilon_2$) were determined with SIESTA program[60] through a single point calculation of the converged geometry of five phases [5-$AVA_{(1-x)}MA_x$]$PbI_3$. The real part of the dielectric constant ($\varepsilon_1$) was extracted from $\varepsilon_2$ using the Kramers-Kronig method.[61] Finally, the frequency-dependent absorption coefficient ($\alpha$) is given by:

$$\alpha(\omega) = \omega\sqrt{\frac{\epsilon_1(\omega) + \sqrt{\epsilon_1(\omega)^2 + \epsilon_2(\omega)^2}}{2}}$$

With this equation, we compared the experimental UV-Vis absorptions curves with the simulated curves of alpha obtained from calculated theoretical models of the five samples of perovskite studied in this work.

The results of the simulated curves obtained from the dielectric function, showed a direct relation of the blue-shift of the absorption coefficient with the systematic increment of 5-AVA ions in the unit cell model (see Fig. 9). However, the phases with x=0.25 and x=0.5 show a very small shift (<0.2 eV) respect to the reference curve of $MAPbI_3$. The calculated curves show less blue-shift that other modified perovskites used to improve stability, like for example, the substitution of iodine by chloride or iodine by bromide.[23] This result indicates that the substitution of MA by 5-AVA in low quantities can maintain the optical properties similar to the original $MAPbI_3$ perovskites, improving the global stability of the crystal, as was previously shown.

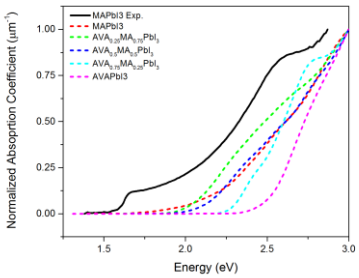


**Figure 9.** Simulated curves of the absorption coefficient calculated for the five phases of [5-$AVA_{(1-x)}MA_x$]$PbI_3$ (short dashed lines) compared with our UV-Vis spectrum of $MAPbI_3$ (black line).

## Conclusions

In summary, we generate a series of five [5-$AVA_{(1-x)}MA_x$]$PbI_3$ samples with a well-established procedure which resulted in a reliable sample to perform measures of XRD and UV-Vis absorptions. The XRD results show the coexistence of the $MAPbI_3$ and 5-$AVAPbI_3$ phases and a well-defined transition between the samples. The same behaviour is obtained from the absorption spectra, resulting in promising optical bandgaps of 1.58 eV for $MAPbI_3$ and 2.33 eV for 5-$AVAPbI_3$. Using theoretical calculations, we found reliable agreement between the experimentally measured bandgaps and the calculated values, for the pure phases. By contrast, poor agreement for the transition samples was found. On the other hand, a direct relationship between the cell stability (through the growth of cohesive energy) and the 5-AVA rate of substitution was found, also tightly related to the systematic increment of the theoretical bandgaps. The DOS and pDOS of the samples showed that apparently, the presence of atomic orbitals of 5-AVA in the CB zone closed to the Fermi level provokes a larger bandgap, which could be attributed to a less

reactivity of the perovskite with respect to the other derivatives[62-64]. Finally, this work shows that the moderated substitution of MA ion by 5-AVA ions in perovskite lead-based solar cells allows modulating several key aspects of the cell with the purpose to drive eventually the design of new materials.

## Conflicts of interest

There are no conflicts to declare.

## Acknowledgements

We are thankful for the financial support from USACH under the Project POSTDOC_DICYT, Código 021941CJ_POSTDOC (R.U.-L., G.C.-J.) Powered@NLHPC: This research was partially supported by the supercomputing infrastructure of the NLHPC (ECM-02) of the Universidad de Chile. M.L.C. and H.X. acknowledge the support from Spanish MINECO for the grants ENE2016-79282-C5-2-R and PID2019-104272RB-C54 the OrgEnergy Excellence Network CTQ2016-81911- REDT, the Agència de Gestiód'Ajuts Universitaris i de Recerca (AGAUR) for the support to the consolidated Catalonia research group 2017 SGR 329 and the Xarxa de Referència en Materials Avançats per a l'Energia (Xarmae). ICN2 is supported by the Severo Ochoa program from Spanish MINECO (Grant No. SEV-2017-0706) and is funded by the CERCA Programme / Generalitat de Catalunya.

## Notes and references

1. A. Kojima, K. Teshima, Y. Shirai and T. Miyasaka, *J. Am. Chem. Soc.*, 2009, **131**, 6050-6051.
2. E. H. Jung, N. J. Jeon, E. Y. Park, C. S. Moon, T. J. Shin, T.-Y. Yang, J. H. Noh and J. Seo, *Nature*, 2019, **567**, 511-515.
3. M. A. Green, E. D. Dunlop, J. Hohl-Ebinger, M. Yoshita, N. Kopidakis and A. W. Y. Ho-Baillie, *Progress in Photovoltaics: Research and Applications*, 2019, **28**, 3-15.
4. F. Sahli, J. Werner, B. A. Kamino, M. Bräuninger, R. Monnard, B. Paviet-Salomon, L. Barraud, L. Ding, J. J. Diaz Leon, D. Sacchetto, G. Cattaneo, M. Despeisse, M. Boccard, S. Nicolay, Q. Jeangros, B. Niesen and C. Ballif, *Nature materials*, 2018, **17**, 820-826.
5. X. Li, M. Ibrahim Dar, C. Yi, J. Luo, M. Tschumi, S. M. Zakeeruddin, M. K. Nazeeruddin, H. Han and M. Grätzel, *Nature Chemistry*, 2015, **7**, 703-711.
6. T.-B. Song, Q. Chen, H. Zhou, S. Luo, Y. M. Yang, J. You and Y. Yang, *Nano Energy*, 2015, **12**, 494-500.
7. Z. Xiao, Y. Yuan, Q. Wang, Y. Shao, Y. Bai, Y. Deng, Q. Dong, M. Hu, C. Bi and J. Huang, *Materials Science and Engineering: R: Reports*, 2016, **101**, 1-38.
8. S. Yang, W. Fu, Z. Zhang, H. Chen and C.-Z. Li, *J. Mater. Chem. A*, 2017, **5**, 11462-11482.
9. K. Zheng, Q. Zhu, M. Abdellah, M. E. Messing, W. Zhang, A. Generalov, Y. Niu, L. Ribaud, S. E. Canton and T. Pullerits, *J. Phys. Chem. Lett.*, 2015, **6**, 2969-2975.
10. H.-S. Kim, C.-R. Lee, J.-H. Im, K.-B. Lee, T. Moehl, A. Marchioro, S.-J. Moon, R. Humphry-Baker, J.-H. Yum, J. E. Moser, M. Grätzel and N.-G. Park, *Journal*, 2012, **2**, 583-587.
11. M. V. Khenkin, E. A. Katz, A. Abate, G. Bardizza, J. J. Berry, C. Brabec, F. Brunetti, V. Bulović, Q. Burlingame, A. Di Carlo, R. Cheacharoen, Y.-B. Cheng, A. Colsmann, S. Cros, K. Domanski, M. Dusza, C. J. Fell, S. R. Forrest, Y. Galagan, D. Di Girolamo, M. Grätzel, A. Hagfeldt, E. von Hauff, H. Hoppe, J. Kettle, H. Köbler, M. S. Leite, S. Liu, Y.-L. Loo, J. M. Luther, C.-Q. Ma, M. Madsen, M. Manceau, M. Matheron, M. McGehee, R. Meitzner, M. K. Nazeeruddin, A. F. Nogueira, Ç. Odabaşı, A. Osherov, N.-G. Park, M. O. Reese, F. De Rossi, M. Saliba, U. S. Schubert, H. J. Snaith, S. D. Stranks, W. Tress, P. A. Troshin, V. Turkovic, S. Veenstra, I. Visoly-Fisher, A. Walsh, T. Watson, H. Xie, R. Yıldırım, S. M. Zakeeruddin, K. Zhu and M. Lira-Cantu, *Nature Energy*, 2020, **5**, 35-49.
12. A. Pérez-Tomás, A. Mingorance, D. Tanenbaum and M. Lira-Cantú, in *The Future of Semiconductor Oxides in Next-Generation Solar Cells*, ed. M. Lira-Cantu, Elsevier, 2018, DOI: https://doi.org/10.1016/B978-0-12-811165-9.00008-9, pp. 267-356.
13. Y. Reyna, A. Pérez-Tomás, A. Mingorance and M. Lira-Cantú, in *Molecular Devices for Solar Energy Conversion and Storage*, eds. H. Tian, G. Boschloo and A. Hagfeldt, Springer Singapore, Singapore, 2018, DOI: 10.1007/978-981-10-5924-7_13, pp. 477-531.
14. Y. Reyna, M. Salado, S. Kazim, A. Pérez-Tomas, S. Ahmad and M. Lira-Cantu, *Nano Energy*, 2016, **30**, 570-579.
15. T. A. Berhe, W.-N. Su, C.-H. Chen, C.-J. Pan, J.-H. Cheng, H.-M. Chen, M.-C. Tsai, L.-Y. Chen, A. A. Dubale and B.-J. Hwang, *Energy Environ. Sci.*, 2016, **9**, 323-356.
16. N. K. Noel, S. D. Stranks, A. Abate, C. Wehrenfennig, S. Guarnera, A.-A. Haghighirad, A. Sadhanala, G. E. Eperon, S. K. Pathak, M. B. Johnston, A. Petrozza, L. M. Herz and H. J. Snaith, *Energy Environ. Sci.*, 2014, **7**, 3061-3068.
17. R. Kour, S. Arya, S. Verma, J. Gupta, P. Bandhoria, V. Bharti, R. Datt and V. Gupta, *Global Challenges*, 2019, **3**, 1900050.
18. D. B. Mitzi, C. A. Feild, Z. Schlesinger and R. B. Laibowitz, *Journal of Solid State Chemistry*, 1995, **114**, 159-163.
19. C. Huang, X. Yan, G. Cui, Z. Liu, S. Pang and H. Xu, *CN Pat. CN*, 2014, **103943368**, 23.
20. S. A. Adonin, L. A. Frolova, M. N. Sokolov, G. V. Shilov, D. V. Korchagin, V. P. Fedin, S. M. Aldoshin, K. J. Stevenson and P. A. Troshin, *Advanced Energy Materials*, 2018, **8**, 1701140.
21. A. Fakharuddin, F. Di Giacomo, I. Ahmed, Q. Wali, T. M. Brown and R. Jose, *Journal of Power Sources*, 2015, **283**, 61-67.
22. Y. Wu, W. Chen, Y. Yue, J. Liu, E. Bi, X. Yang, A. Islam and L. Han, *ACS Appl. Mater. Interfaces*, 2015, **7**, 20707-20713.
23. T. Salim, S. Sun, Y. Abe, A. Krishna, A. C. Grimsdale and Y. M. Lam, *J. Mater. Chem. A*, 2015, **3**, 8943-8969.
24. M. Saliba, T. Matsui, J.-Y. Seo, K. Domanski, J.-P. Correa-Baena, M. K. Nazeeruddin, S. M. Zakeeruddin, W. Tress, A. Abate, A. Hagfeldt and M. Grätzel, *Energy Environ. Sci.*, 2016, **9**, 1989-1997.
25. J. W. Lee, D. H. Kim, H.-S. Kim, S. W. Seo, S. M. Cho and N.-G. Park, *Advanced Energy Materials*, 2015, **5**, 1501310.
26. A. Mei, X. Li, L. Liu, Z. Ku, T. Liu, Y. Rong, M. Xu, M. Hu, J. Chen, Y. Yang, M. Grätzel and H. Han, *Science*, 2014, **345**, 295-298.

**Formatted:** Font: (Default) Calibri, 12 pt, Do not check spelling or grammar, Character scale: 100%

27. G. Grancini, C. R. a. n-Carmona, I. Zimmermann, E. Mosconi, X. Lee, D. Martineau, S. Narbey, F. Oswald, F. De Angelis, M. Graetzel and M. K. Nazeeruddin, *Nature Communications*, 2017, **8**, 1-8.
28. M. Lira-Cantú, *Nature Energy*, 2017, **2**, 17115.
29. M. L.-C. Editor, *The Future of Semiconductor Oxides in Next-Generation Solar Cells*, Elsevier Ghenadii Korotcenkov, Metal Oxides Series Editor, 2017.
30. N. Ashari-Astani, F. Jahanbakhshi, M. Mladenović, A. Q. M. Alanazi, I. Ahmadabadi, M. R. Ejtehadi, M. I. Dar, M. Grätzel and U. Rothlisberger, *The Journal of Physical Chemistry Letters*, 2019, **10**, 3543-3549.
31. A. Q. Alanazi, D. J. Kubicki, D. Prochowicz, E. A. Alharbi, M. E. F. Bouduban, F. Jahanbakhshi, M. Mladenović, J. V. Milić, F. Giordano, D. Ren, A. Y. Alyamani, H. Albrithen, A. Albadri, M. H. Alotaibi, J.-E. Moser, S. M. Zakeeruddin, U. Rothlisberger, L. Emsley and M. Grätzel, *Journal of the American Chemical Society*, 2019, **141**, 17659-17669.
32. T. Baikie, Y. Fang, J. M. Kadro, M. Schreyer, F. Wei, S. G. Mhaisalkar, M. Graetzel and T. J. White, *J. Mater. Chem. A*, 2013, **1**, 5628-5614.
33. W. Kohn and L. J. Sham, *Physical Review*, 1965, **140**, A1133-A1138.
34. J. P. Perdew, K. Burke and M. Ernzerhof, *Phys. Rev. Lett.*, 1996, **77**, 3865-3868.
35. P. Giannozzi, S. Baroni, N. Bonini, M. Calandra, R. Car, C. Cavazzoni, D. Ceresoli, G. L. Chiarotti, M. Cococcioni, I. Dabo, A. Dal Corso, S. de Gironcoli, S. Fabris, G. Fratesi, R. Gebauer, U. Gerstmann, C. Gougoussis, A. Kokalj, M. Lazzeri, L. Martin-Samos, N. Marzari, F. Mauri, R. Mazzarello, S. Paolini, A. Pasquarello, L. Paulatto, C. Sbraccia, S. Scandolo, G. Sclauzero, A. P. Seitsonen, A. Smogunov, P. Umari and R. M. Wentzcovitch, *J. Phys.: Condens. Matter*, 2009, **21**, 395502.
36. S. Grimme, J. Antony, S. Ehrlich and H. Krieg, *The Journal of Chemical Physics*, 2010, **132**, 154104.
37. P. E. Blöchl, *Physical Review B*, 1994, **50**, 17953-17979.
38. H. J. Monkhorst and J. D. Pack, *Physical Review B*, 1976, **13**, 5188-5192.
39. G. te Velde, F. M. Bickelhaupt, E. J. Baerends, C. Fonseca Guerra, S. J. A. van Gisbergen, J. G. Snijders and T. Ziegler, *Journal of Computational Chemistry*, 2001, **22**, 931-967.
40. P. H. T. Philipsen, G. te Velde, E. J. Baerends, J. A. Berger, P. L. de Boeij, M. Franchini, J. A. Groeneveld, E. S. Kadantsev, R. Klooster, F. Kootstra, P. Romaniello, M. Raupach, D. G. Skachkov, J. G. Snijders, C. J. O. Verzijl, J. A. C. Gil, J. M. Thijssen, G. Wiesenekker and T. Ziegler.
41. Y. Yamada, T. Yamada, L. Q. Phuong, N. Maruyama, H. Nishimura, A. Wakamiya, Y. Murata and Y. Kanemitsu, *Journal of the American Chemical Society*, 2015, **137**, 10456-10459.
42. M. Yang, T. Zhang, P. Schulz, Z. Li, G. Li, D. H. Kim, N. Guo, J. J. Berry, K. Zhu and Y. Zhao, *Nature Communications*, 2016, **7**, 12305.
43. H. Wang, Z. Wang, Z. Yang, Y. Xu, Y. Ding, L. Tan, C. Yi, Z. Zhang, K. Meng, G. Chen, Y. Zhao, Y. Luo, X. Zhang, A. Hagfeldt and J. Luo, *Advanced Materials*, 2020, **32**, 2000865.
44. D. Bi, C. Yi, J. Luo, J.-D. Décoppet, F. Zhang, Shaik M. Zakeeruddin, X. Li, A. Hagfeldt and M. Grätzel, *Nature Energy*, 2016, **1**, 16142.
45. R. Lindblad, D. Bi, B.-w. Park, J. Oscarsson, M. Gorgoi, H. Siegbahn, M. Odelius, E. M. J. Johansson and H. Rensmo, *The Journal of Physical Chemistry Letters*, 2014, **5**, 648-653.
46. D. H. Cao, C. C. Stoumpos, O. K. Farha, J. T. Hupp and M. G. Kanatzidis, *Journal of the American Chemical Society*, 2015, **137**, 7843-7850.
47. Y. Jiang, M. A. Green, R. Sheng and A. Ho-Baillie, *Solar Energy Materials and Solar Cells*, 2015, **137**, 253-257.
48. S. Tombe, G. Adam, H. Heilbrunner, D. H. Apaydin, C. Ulbricht, N. S. Sariciftci, C. J. Arendse, E. Iwuoha and M. C. Scharber, *J. Mater. Chem. C*, 2017, **5**, 1714-1723.
49. N. Kitazawa, Y. Watanabe and Y. Nakamura, *Journal of Materials Science*, 2002, **37**, 3585-3587.
50. Y. Jiang, M. A. Green, R. Sheng and A. Ho-Baillie, 2016, 1-8.
51. A. Poglitsch and D. Weber, *The Journal of Chemical Physics*, 1987, **87**, 6373-6378.
52. E. Menéndez-Proupin, P. Palacios, P. Wahnón and J. C. Conesa, *Phys. Rev. B*, 2014, **90**, 3586-3587.
53. D. Liu, S. Li, F. Bian and X. Meng, *Materials 2010, Vol. 3, Pages 1709-1745*, 2018, **11**, 1141-1111.
54. U.-G. Jong, C.-J. Yu, Y.-M. Jang, G.-C. Ri, S.-N. Hong and Y.-H. Pae, *Journal of Power Sources*, 2017, **350**, 65-72.
55. G. Kieslich, S. Sun and A. K. Cheetham, *Chemical Science*, 2014, **5**, 4712-4715.
56. S. Tao, I. Schmidt, G. Brocks, J. Jiang, I. Tranca, K. Meerholz and S. Olthof, *Nature Communications*, 2019, DOI: papers3://publication/doi/10.1038/s41467-019-10468-7, 1-10.
57. L. Zhou, A. J. Neukirch, D. J. Vogel, D. S. Kilin, L. Pedesseau, M. A. Carignano, A. D. Mohite, J. Even, C. Katan and S. Tretiak, *ACS Energy Letters*, 2018, **3**, 787-793.
58. E. Mosconi, P. Umari and F. De Angelis, *Physical Chemistry Chemical Physics*, 2016, **18**, 27158-27164.
59. C. C. Boyd, R. Cheacharoen, T. Leijtens and M. D. McGehee, *Chem Rev*, 2019, **119**, 3418-3451.
60. M. S. José, A. Emilio, D. G. Julian, G. Alberto, J. Javier, O. Pablo and S.-P. Daniel, *J. Phys.: Condens. Matter*, 2002, **14**, 2745.
61. K. E. Peiponen and J. J. Saarinen, *Reports on Progress in Physics*, 2009, **72**, 056401.
62. R. G. Parr and Y. Weitao, *Density-Functional Theory of Atoms and Molecules*, Oxford University Press, 1989.
63. R. G. Pearson, *Journal of the American Chemical Society*, 1985, **107**, 6801-6806.
64. R. G. Parr and R. G. Pearson, *Journal of the American Chemical Society*, 1983, **105**, 7512-7516.